

TOTAL ABSORPTION COEFFICIENTS OF AIR HEATED BY STRONG SHOCK WAVES

A. I. PETRUKHIN and V. A. PROSKURYAKOV

Institute of Physics of the Earth, Academy of Sciences, U.S.S.R.

Submitted to JETP editor June 15, 1966

J. Exptl. Theoret. Phys. (U.S.S.R.) 51, 1348-1357 (November, 1966)

The emissive power of air is investigated at temperatures from 13 000 to 65 000° K. A powerful spark discharge created shock waves in a tube. The law of motion of the shock front for initial air pressures from 0.1 to 500 mm Hg is established. The temperature and charged particle distributions behind the shock front are measured optically at initial pressures of 0.1, 0.2, and 0.5 mm Hg, and small regions are found (with dimensions of 1.5-2 cm) in which the plasma parameters are close to their equilibrium values. Radiative losses of the plasma in the equilibrium region adjacent to the front are calculated on the basis of the measured temperature and density distributions. The total absorption coefficients of the plasma are determined.

1. INTRODUCTION

SHOCK waves having velocities of tens or even hundreds of kilometers per second can be produced in electromagnetic shock tubes. In these devices gas temperatures behind the shock front reach tens or even hundreds of thousands of degrees. The gasdynamical processes occurring at such temperatures are strongly influenced by radiation. In electromagnetically driven shock tubes high velocities and temperatures are usually realized at relatively low gas densities, where the radiation mean free path is usually much greater than the dimensions of the disturbed region. Under these conditions the radiation merely transfers energy from the shock wave to the tube walls and the gas flow behind the front becomes essentially nonadiabatic.

Nonadiabaticity of the flow affects primarily the damping of shock waves, and induces a considerably steeper decrease of shock front velocity along a tube than in the adiabatic case. The temperature, density, and pressure distributions behind the front are also affected. Radiation changes these conditions to a lesser degree at the shock front.

If the relaxation zone has small dimensions and radiation out of this region does not strongly affect the energy of gas traversing the region, the Rankine-Hugoniot conditions for shock fronts remain the same as in the case of adiabatic flow. Therefore, for the purpose of investigating gasdynamical processes in strong shock waves we must know the emissive powers of gases heated to high temperatures.

The radiative properties of hot gases are important for many physical and gasdynamical processes in high-temperature gases as well as specifically for shock waves. Therefore the determination of the emissive power possesses independent interest. However both the theoretical calculations and experimental measurements of the emissive power encounter considerable difficulties that result from the diversity and complexity of high-temperature gas processes.

The greatest experimental difficulties arise in the production of plasmas having the requisite parameters. Great experimental difficulties are also associated with the complexity of the radiation spectrum. At tens or hundreds of thousands of degrees a considerable fraction of the plasma radiation energy lies in the far ultraviolet and soft x-ray regions, where optical measurements require a highly refined and complicated technique.

Information concerning the total emissive power of a hot gas can sometimes be derived by studying the gasdynamical flow parameters in strong shock waves. If the gas behind a shock front is in a state of local thermodynamic equilibrium, the flow behind the front is described by the conventional gasdynamical equations. Specifically, energy conservation is described by the equation

$$\frac{\partial e}{\partial t} + u \frac{\partial e}{\partial r} + p \left(\frac{\partial v}{\partial t} + u \frac{\partial v}{\partial r} \right) = -f; \quad (1)$$

here e is the energy per mass unit, u is the flow speed, p is the pressure, $v = 1/\rho$ is the specific volume, ρ is the gas density, and f is the energy loss per mass unit in a unit of time.

The energy and pressure are functions of the temperature and density (or specific volume): $e = e(T, v)$ and $p = p(T, v)$. Therefore, when the temperature and density distributions behind the front have been measured, Eq. (1) can be used to calculate f , which receives its main contribution from the radiation. The problem becomes considerably simpler when we know the law of motion in any flow region behind the front that possesses known gasdynamical parameters. It has been shown^[1] that in this case the gasdynamical equations yield derivatives of the flow parameters with respect to the mass-position coordinate, which are expressed in terms of the known values for the aforementioned region and the specific energy loss f .

It follows from the equations that f can be determined by measuring the derivative with respect to the mass-position coordinate for a single parameter of flow behind the front (temperature, density, or pressure). However, the experimental determination of the distributions of these parameters with respect to the mass-position coordinate is considerably more complicated than plotting the time dependences of these quantities at fixed points in the flow behind the front. It is therefore advantageous to obtain f in terms of the time derivative of a flow parameter; this can be done by the method that was used in^[1].

If the relaxation zone behind a compression shock front is small and emits little radiation, then the required region that is subject to a known law of motion and has known parameters can be the region of thermodynamic equilibrium immediately adjacent to the front. We shall now determine f for this zone. The customary equations of motion for a nonstationary one-dimensional flow are

$$\frac{\partial v}{\partial t} + u \frac{\partial v}{\partial r} - v \frac{\partial u}{\partial r} = \frac{v-1}{r} v u, \quad \frac{\partial u}{\partial t} + u \frac{\partial u}{\partial r} + v \frac{\partial p}{\partial r} = 0, \quad (2)$$

where r is the distance from the detonation source, and $\nu = 1, 2, 3$ for plane, cylindrical, and spherical flow symmetry, respectively.

Let $r = R(t)$ be the law of motion of the shock front, where R is the coordinate of the front. Using the symbolic identity $d/dR = \partial/\partial r + D^{-1}\partial/\partial t$, where D is the shock front velocity, we eliminate the derivatives with respect to the coordinate from (1) and (2). Then, using the relations at the front:

$$p_s - p_0 = D^2 v_0^{-1} (v_0 - v_s), \quad e_s - e_0 = \frac{1}{2} (p_s + p_0) (v_0 - v_s), \\ u = D(1 - v_s/v_0), \quad (3)$$

to calculate the derivatives d/dR , we obtain by means of simple transformations

$$-f = A \frac{dD}{dR} + B \frac{\partial T}{\partial t} + C, \quad (4)$$

where

$$A = \frac{[(\partial e/\partial v)_T + p_s]}{D/v_0 + v_0 D^{-1}(\partial p/\partial v)_T} \\ \times \left[(1-\gamma)(1+2\gamma)D + 2D^2 \frac{d\gamma}{dD} \right] + (1-\gamma)^2 D^2, \\ B = \gamma \left(\frac{\partial e}{\partial T} \right)_v - \gamma \frac{v_0}{D} \left(\frac{\partial p}{\partial T} \right)_v \\ \times \left[\left(\frac{\partial e}{\partial v} \right)_T + p_s \right] / \left[\frac{D}{v_0} + \frac{v_0}{D} \left(\frac{\partial p}{\partial v} \right)_T \right], \\ C = \left[\left(\frac{\partial e}{\partial v} \right)_T + p_s \right] \left[\frac{D}{v_0} + \frac{v_0}{D} \left(\frac{\partial p}{\partial v} \right)_T \right]^{-1} \frac{v-1}{R} D^2 \gamma (1-\gamma). \quad (4a)$$

Here $\gamma = v_s/v_0$; the index s denotes parameters at the front; the index 0 denotes parameters ahead of the front.

In Eq. (4), f depends on $\partial T/\partial t$; similar equations can be derived in terms of $\partial p/\partial t$ or $\partial v/\partial t$. Equation (4) shows that in order to determine f the dependence of the shock front velocity on distance must be measured, as well as the temporal variation of temperature at some point for a known velocity of the front. The other quantities in these equations can be calculated from the equations of state and from the conditions at the front.

We have previously shown^[2] that air behind a strong shock created by a spark discharge in a tube is in a near-equilibrium state and satisfies the Rankine-Hugoniot conditions. In virtue of the foregoing discussion, we can in this case use (4) to calculate the specific energy loss of air that is heated by a shock wave to a few tens of thousands of degrees.

In the present work we present measurements of shock front velocity in an electromagnetically driven tube as a function of distance from the discharge gap, and of the temperature and density distributions behind the front. These measurements then serve as a basis for calculating the emissive power of air under the experimental conditions.

2. INVESTIGATION OF THE LAW OF MOTION OF SHOCK WAVES

For the purpose of determining the law of motion of the shock waves we measured simultaneously the shock front velocity at different distances from the discharge gap and the energy released by

the discharge. The experimental work was done with the same apparatus that we have described in [2, 3] at a constant potential of 16 kV on the battery of condensers. The spark gap was located in the end face of a steel tube that consisted of four interchangeable sections with a total length of 2 m. The inside diameter of the tube was ≈ 110 mm. The electrodes were a brass ring and a rod positioned coaxially. To fix the spark gap, both the ring and the rod were provided with projections, the gap between the latter being ≈ 6 mm. Following each shot the tube was refilled with air to atmospheric pressure and was then reevacuated to the required initial pressure.

In order to measure the energy released in the spark gap oscillograms of the current and voltage in the gap were recorded; typical examples are shown in Fig. 1. The highly damped oscillatory discharge had a period $\sim 17 \mu\text{sec}$. The maximum current during the first half-period was 3×10^5 A and the average rate of energy release was $(2-3) \times 10^{15}$ erg/sec. The simultaneous currents and voltages on the oscillograms were multiplied together to provide curves of the power released in the spark gap; the curves were integrated graphically. At initial air pressures from 0.1 to 500 mm the energy released in the spark gap was only slightly dependent on the pressure. The average total energy was about 3000 J, 80% of which was released during the first half-period of the discharge ($8.5 \mu\text{sec}$). Control experiments performed with magnetic probes showed that plasmoids and filamentary currents were not observable at distances ≥ 26 cm from the spark gap.

Shock wave velocities were measured at distances of 26, 85, 146, and 197 cm from the spark gap by high-speed schlieren photography of the luminous shock front using an SFR-2m camera.

Since the depth of the observed object was only ~ 110 mm the schlieren apparatus was set up with

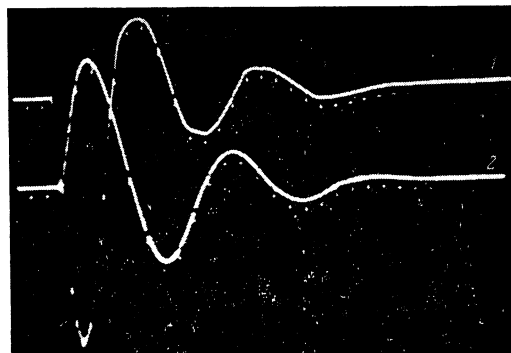


FIG. 1. Current and voltage in the spark gap. 1 – voltage, 2 – current. Time markings 2 μsec apart.

a single spherical mirror that directed a convergent light beam through the experimental object. The light-source gap and knife edge of the system were located at distances equal to twice the focal length of the mirror. The function of the knife edge was performed by the entrance diaphragm of the SFR camera, which was operated as a two-lens framing camera. Figure 2 shows the optical scheme of the schlieren cinematography. Figure 3 shows typical schlieren photographs of one experiment; the shock front appears clearly in a series of frames. These photographs were obtained in the case of 4-mm initial air pressure with the distance $R = 85$ cm between the spark gap and the center of the window. The shock front velocity was 2.4 km/sec. We do not completely understand the nature of the light that was removed from the front by the dark space.

It was determined from the schlieren cinematography and shock speed measurements that at speeds ≥ 6 km/sec ($M \geq 18$) the luminous front coincides (within the 2-4-mm experimental accuracy limits) with the viscous compression shock, independently of the distance from the discharge gap.

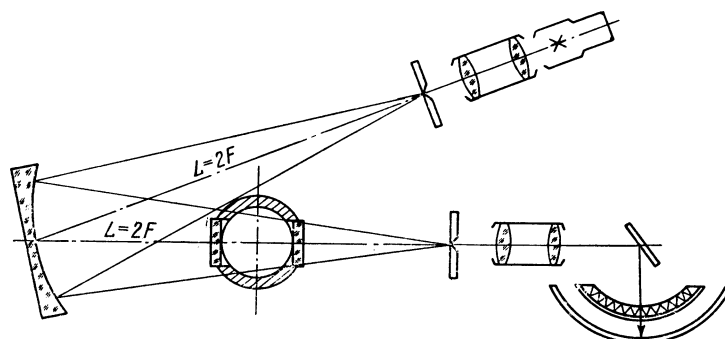


FIG. 2. Optical arrangement of the schlieren cinematography.

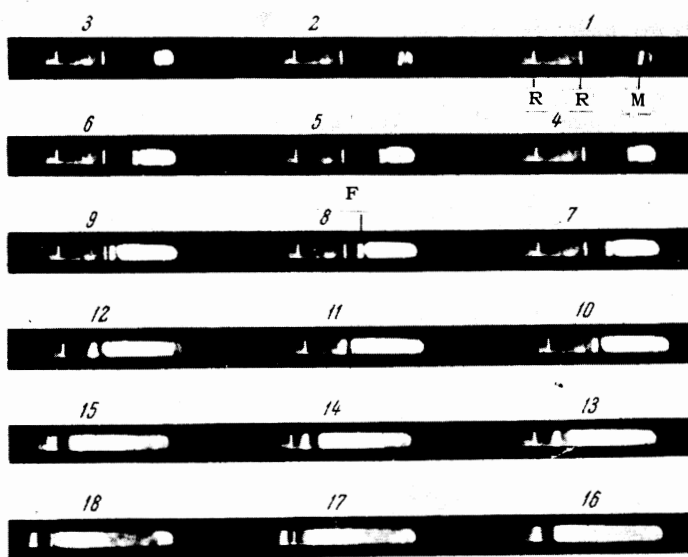


FIG. 3. Schlieren photographs of shock wave. $R = 85$ cm, $P_0 = 4.0$ mm Hg, shock front velocity $D = 2.42$ km/sec; F is the shock front, P is a reference line, and M is the luminous mirror edge. The separation of the reference lines is 62 mm.

In the high-speed photographs used to measure velocities the light wave front coincided with the shock front. Figure 4 is a photograph of a luminous shock wave; a region of almost uniform brightness, 1.5–2 cm wide, is clearly visible immediately adjacent to the front.

Figure 5 shows the dependence of the measured shock velocities on the experimental conditions. Here $M = D/c_0$, where D is the front velocity at a distance R from the spark gap; c_0 is the velocity of sound in undisturbed air; $l = P_0SR/E_{1/2}$ is a dimensionless parameter, where $E_{1/2}$ is the energy released in the spark gap during a half-period, P_0 is the initial air pressure in the tube, and S is the cross sectional area of the tube.

We observe that with the exception of the shortest distance from the discharge ($R = 26$ cm) all experimental results fit well on a common curve (10% accuracy was estimated for the velocity measurements). This indicates that the fraction of the discharge energy expended in forming the shock

wave is independent of the initial pressure in the tube; otherwise the experimental results for different pressures would lie on different curves. It appears that the shock wave is still being formed up to $R = 26$ cm, i.e., the motion of the shock here still depends on the properties of the source, so that the experimental results for this distance lie on different curves. The dot-dash line that is shown for comparison describes the propagation of a shock wave in the case of a strong planar detonation^[4] having 25% of the energy actually released during the first half-period of the discharge. This curve agrees well with experiment below $M = 20$ ($D \approx 7$ km/sec).

The high-speed shock waves ($M > 20$) are damped at distances $R \geq 85$ cm from the spark gap much more strongly than one would expect from the propagation law for strong-detonation shock waves. Similar results were obtained in^[5] in the case of an electromagnetically-driven shock tube with a conical discharge space, at 0.03 mm initial air pressure.

3. TEMPERATURE AND DENSITY DISTRIBUTIONS BEHIND THE SHOCK FRONT

For temperature measurements we employed a method involving the relative intensities of two spectral lines with known oscillator strengths. The collimated light beam from a moving shock wave was split into two beams by a semitransparent mirror; the two beams passed through two different monochromators and entered photomultipliers whose signals were registered by a double-beam oscillograph. The simultaneous registration of

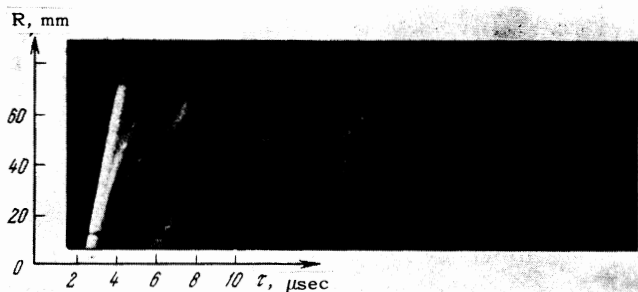


FIG. 4. Streak photograph of shock wave. $P_0 = 0.1$ mm Hg, $D = 48$ km/sec. The time markers are 2 μ sec apart.

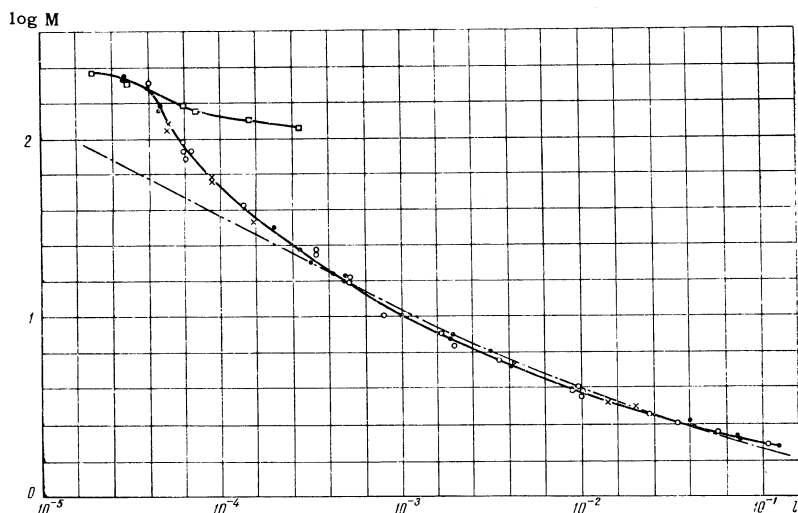


FIG. 5. Dependence of shock wave velocity on experimental conditions. $M = D/c_0$ (c_0 is the velocity of sound in undisturbed air), \square - $R = 26$ cm, \bullet - $R = 85$ cm, \circ - $R = 146$ cm, \times - $R = 197$ cm.

two line intensities enabled us to plot a time curve of the gas temperature behind the shock front at a fixed distance from the discharge; several pairs of lines belonging to atomic and ionized nitrogen were used for this purpose.

Gas densities were calculated from the measured concentrations of charged particles in the plasma behind the shock front. The same monochromator system was used to plot $H\beta$ line shapes averaged over several identical experiments. The $H\beta$ line shapes plotted for different times following the passage of the shock front through the observation point enabled us to calculate the concentrations of charged particles.^[6, 7] On the basis of these concentrations together with the measured temperature distributions and thermodynamic tables for air^[8] we calculated the gas density distribution behind the shock front. A detailed account of the measuring technique and treatment of the results has appeared in^[2].

Figures 6 and 7 show the measured temperature and gas density distributions behind the shock front at 85 cm from the spark gap for initial air pressures of 0.1, 0.2, and 0.5 mm. It should be noted that at the initial pressure $P_0 = 0.1$ mm the time dependences of T/T_s and ρ/ρ_s (where T_s and ρ_s are the temperature and density at the wave front) coincided within experimental accuracy limits for the two distances from the spark gap, 85 and 142 cm, at which measurements were obtained.

A region of 1-2 cm near the front exhibits approximately uniform temperature and density according to Figs. 6 and 7. We have previously shown^[2] that in this region the state of the gas satisfies the Rankine-Hugoniot conditions.

4. CALCULATION OF ENERGY LOSS FOR HEATED GAS LAYER AT A SHOCK FRONT

The gas temperature and density measurements behind the shock front show that in our case the conditions satisfied Eq. (4) for the specific energy loss rate of the air layer adjacent to the front. The derivatives appearing in (4) were calculated by using simple step functions to extrapolate the ex-

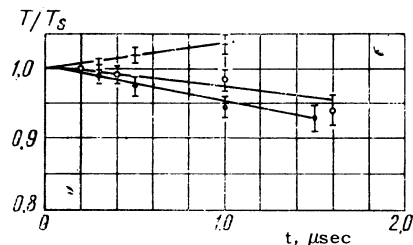


FIG. 6. Temperature distribution behind a shock front. $R = 85$ cm, P_0 in mm Hg: \bullet - 0.1, \circ - 0.2, \times - 0.5.

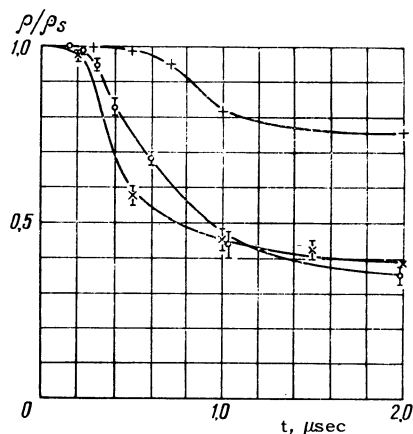


FIG. 7. Density distribution behind a shock front. $R = 85$ cm, P_0 in mm Hg: \times - 0.1, \circ - 0.2, \times - 0.5.

perimental dependences and the equation of state.

The law of motion of a shock front within the velocity limits considered by us permits good extrapolation (for 10% experimental accuracy) by the expression $D = A/R$, where the constant A depends on the initial air pressure in the tube. The temperature distribution was extrapolated by means of the linear equation $T/T_s = 1 - at$, where the constant a depends on P_0 . Kuznetsov's tables^[8] were used to extrapolate the density and temperature dependences of the internal energy of air. Table I gives the results of calculations based on (4).

Under our experimental conditions the main contribution to f comes from the first term on the right-hand side of (4), and is approximately one order of magnitude greater than the contribution of the second term. Therefore the extrapolation for T/T_s does not require great accuracy, and for the same reason the errors of air temperature distribution measurements behind the shock front have practically no effect on the accuracy of the f values.

The specific energy loss can be calculated from the experimentally measured density distribution behind the front. As already stated in our Introduction, an expression for f that resembles (4) is obtained in this case. However, Fig. 7 shows that the experimental time derivative of the density may be very approximate, thus leading to a large error of f . While the calculation based on (4) yields about 40% error for f , the calculation based on the derivative of density can yield a result that is accurate only to within the factor 2. Nevertheless, the latter calculation was performed as a control, yielding results that differed from those in Table I by at most the factor 2. Therefore the values of f calculated from the temperature distribution and from the density distribution agree within the limits of experimental accuracy.

Among the possible mechanisms of plasma energy losses behind a shock front, radiation cooling and thermal conduction are the most important. Since we are here considering only a narrow region of heated gas immediately adjacent to the

shock front, the boundary layer has only a small influence. Since the measured frontal temperature practically agrees with the temperature calculated from the shock adiabatic curve, we do not expect to find appreciable radial temperature gradients. This inference is confirmed by direct calculations of temperature distributions in shock tubes.^[9] Therefore thermal conduction can cause appreciable thermal energy loss only along the tube axis.

To evaluate the energy loss per unit volume of the postfrontal plasma we write the thermal conduction equation for the plane case in the coordinate frame of the flow:

$$q = \frac{\partial}{\partial r} \left(k_e \frac{\partial T}{\partial r} \right), \quad (5)$$

where k_e is the electronic thermal conductivity and q is the rate of thermal loss per unit gas volume.

The time derivative of temperature can be expressed through the derivative with respect to the coordinate:

$$\frac{\partial}{\partial r} = \frac{dt}{dr} \frac{\partial}{\partial t} = \frac{1}{u} \frac{\partial}{\partial t}, \quad (6)$$

where u is the flow speed. Making this substitution in (5) and taking from^[10] the electronic thermal conductivity coefficient $k_e = \alpha T^{5/2}$, where $\alpha = 1.7 \times 10^{-6}$ erg/cm-sec ($^\circ K$)^{7/2}, we obtain

$$q = 1.7 \cdot 10^{-6} \frac{1}{u^2} \left[\frac{5}{2} T^{3/2} \left(\frac{\partial T}{\partial t} \right)^2 + T^{5/2} \frac{\partial^2 T}{\partial t^2} \right], \quad (7)$$

which under the most severe conditions—shock front velocity $D \approx 50$ km/sec and $T \approx 70\,000$ K—yields $q = 10^8$ erg/cm³-sec. This comprises less than 0.01% of the total energy loss. It therefore appears that the energy loss of the plasma in a narrow region directly behind the front results mainly from radiation cooling. The quantity $f\rho_s$ is then simply the total emissive power per unit volume of the plasma, which is related to the total absorption coefficient κ by the equation $\kappa = f\rho_s/4\sigma T^4$,^[11] where σ is the Stefan-Boltzmann constant.

Total absorption coefficients calculated from the data in Table I are given in Table II, together

Table I

P_0 , mm Hg	R, cm	$D \times 10^{-6}$, cm/sec	$T_s \cdot 10^{-3}$, $^\circ K$	$e_s \times 10^{-10}$ erg/g	$10^{-4} a$, sec ⁻¹	$\frac{1}{\gamma} = \frac{v_0}{v_s}$	$10^{-11} f\rho_s$, erg/cm ³ -sec
0,1	85	4,8	65,0	990	7	14,1	10 (2,80 ± 1)
0,1	142	2,88	33,6	360	7	14,8	3,7 ± 1,5
0,2	85	2,6	31,7	292	5	14,2	7,1 ± 3
0,2	142	1,6	15,4	114	0	16,9	1,0 ± 0,4
0,5	85	1,25	13,3	68	-5	15,6	1,1 ± 0,4

Table II

$10^{-3} T, ^\circ K$	$10^3 \delta = 10^3 \frac{\rho_s^*}{\rho_{norm}}$	$10^{-11} f \rho_s, \frac{erg}{cm^2 \cdot sec}$	κ_{exp}, cm^{-1}	κ_{theor}, cm^{-1}
65.0	1.8	28	$5.4 \cdot 10^{-4}$	$1.9 \cdot 10^{-3}$
33.6	1.9	3.7	$1.3 \cdot 10^{-3}$	$3.6 \cdot 10^{-3}$
31.7	3.5	7.1	$3.3 \cdot 10^{-3}$	$9.8 \cdot 10^{-3}$
15.4	4.2	1.0	$8.2 \cdot 10^{-3}$	$2.3 \cdot 10^{-2}$
13.3	9.7	1.1	$2.2 \cdot 10^{-2}$	$3.2 \cdot 10^{-2}$

* $\rho_{norm} = 1.3 \times 10^{-3} g/cm^3$ is the density of dry air at atmospheric pressure; ρ_s is the air density immediately behind the wave front.

with the theoretical values taken from Kuznetsov's thermodynamic tables.^[8]

As already mentioned, the temperature and density distributions for $P_0 = 0.1$ mm are identical at 85 and 142 cm from the discharge. If it is assumed that the distributions have these same values uniformly at all intermediate distances, the total absorption coefficients can be calculated for these distances. It is seen in Table II that the measured total absorption coefficients differ from the theoretical values by a factor not exceeding three or four.

If it is assumed that the theoretical absorption coefficients in^[8] are accurate to within the order of magnitude while the error of κ is estimated at 60%, good agreement between theory and experiment must be acknowledged. Thus, if the foregoing conditions are fulfilled the total absorption coefficients of high-temperature gases can be determined from measurements of gasdynamical parameter distributions behind the front of a strong shock wave.

The authors are indebted to I. L. Zel'man for his sustained interest in this work and for valuable comments, as well as to N. M. Kuznetsov, I. V. Nemchinov, and K. E. Gubkin for useful discussions.

¹V. V. Adushkin and I. V. Nemchinov, PMTF (Applied Mechanics and Technical Physics) No. 4, 58 (1963).

²A. I. Petrukhin and V. A. Proskuryakov, JETP 50, 1481 (1966), Soviet Phys. JETP 23, 986 (1966).

³V. A. Belokon', A. I. Petrukhin, and V. A. Proskuryakov, JETP 48, 50 (1965), Soviet Phys. JETP 21, 33 (1965).

⁴L. I. Sedov, *Metody podobiya i razmernosti v mekhanike* (Similarity and Dimensional Methods in Mechanics), Gostekhizdat, 1954.

⁵H. Guthart and T. Morita, J. Appl. Phys. 36, 2577 (1965).

⁶H. Margenau, in *Proceedings of the Fourth International Conference on Ionization Phenomena in Gases*, Uppsala, 1959, edited by N. R. Nilsson, North-Holland Publ. Co., Amsterdam, 1960, p. 799.

⁷H. Margenau and M. Lewis, *Revs. Modern Phys.* 31, 569 (1959).

⁸N. M. Kuznetsov, *Termodinamicheskie funktsii i udarnye adiabaty vozdukh pri vysokikh temperaturakh* (Thermodynamic Functions and Shock Adiabatic Curves of Air at High Temperatures), Mashinostroenie, 1965.

⁹V. G. Sevast'yanenko and I. T. Yakubov, *Optika i spektroskopiya* 16, 1 (1964).

¹⁰M. Y. Jaffrin and R. F. Probst, *Phys. Fluids* 7, 1658 (1964).

¹¹Ya. B. Zel'dovich and Yu. P. Raizer, *Fizika udarnykh voln i vysokotemperaturnykh gidrodinamicheskikh yavlenii* (Physics of Shock Waves and High-Temperature Hydrodynamic Phenomena), Fizmatgiz, 1963.